Journal of Zhejiang University-SCIENCE A (Applied Physics & Engineering)
ISSN 1673-565X (Print); ISSN 1862-1775 (Online)
www.zju.edu.cn/jzus; www.springerlink.com
E-mail: jzus@zju.edu.cn

Magnetometer-only linear attitude estimation for bias momentum pico-satellite*

Ke HAN, Hao WANG†‡, Zhong-he JIN

(*Department of Information Science and Electronic Engineering, Zhejiang University, Hangzhou 310027, China*)

†E-mail: roger@zju.edu.cn

Received Nov. 14, 2009; Revision accepted Mar. 8, 2010; Crosschecked Apr. 28, 2010

Abstract: Satellite attitude information is essential for pico-satellite applications requiring light-weight, low-power, and fast-computation characteristics. The objective of this study is to provide a magnetometer-only attitude estimation method for a low-altitude Earth orbit, bias momentum pico-satellite. Based on two assumptions, the spacecraft spherical symmetry and damping of body rates, a linear kinematics model of a bias momentum satellite's pitch axis is derived, and the linear estimation algorithm is developed. The algorithm combines the linear Kalman filter (KF) with the classic three-axis attitude determination method (TRIAD). KF is used to estimate satellite's pitch axis orientation, while TRIAD is used to obtain information concerning the satellite's three-axis attitude. Simulation tests confirmed that the algorithm is suited to the time-varying model errors resulting from both assumptions. The estimate result keeps tracking satellite attitude motion during all damping, stable, and free rotating control stages. Compared with nonlinear algorithms, such as extended Kalman filer (EKF) and square root unscented Kalman filer (SRUKF), the algorithm presented here has an almost equal performance in terms of convergence time and estimation accuracy, while the consumption of computing resources is much lower.

Key words: Pico-satellite, Attitude estimation, Bias momentum, Magnetometer, Kalman filter (KF)
doi:10.1631/jzus.A0900725 **Document code:** A **CLC number:** V448.22

1 Introduction

Recently, considerable effort has been invested in research and development programs for micro-technology for space applications (Harmann *et al.*, 2005). Pico-satellite research is one of these programs. The development of a satellite weighing only about 1 kg may significantly reduce space vehicle launch costs, as well as the manufacturing time. By January 2008, more than 30 different pico-satellites had been launched into space (Nugent *et al.*, 2008), and the design complexity of these pico-satellites continues to increase. The trend of pico-satellite research is increasingly directed to practical applications. This leads, however, to a dilemma in pico-satellite design. To operate in practical applications, the satellite needs to have various functions, such as communication, command and data handling, power supply, thermal control, attitude control, etc. This requirement may conflict with the limited design budget of mass, volume, and power in the pico-satellite. Generally, designing a pico-satellite with powerful functions is a very constrained task, as there is a small design margin to guarantee reliability and adaptability.

Attitude determination and control system (ADCS) is one of the key systems in a pico-satellite. The ability of flexible attitude maneuvering may greatly extend a satellite's applicable range. To ensure system reliability, quite a number of pico-satellites adopt passive or semi-passive attitude control designs, such as gravity gradient (Martinelli and Sánchez Peña, 2005), permanent magnet (Funase *et*

‡ Corresponding author

* Project supported by the Program for New Century Excellent Talents in University (No. NCET-06-0514), China, and the Postdoctoral Science Foundation of China (Nos. 20081458 and 20080431306)

al., 2007), bias momentum configuration (Rankin, 2005; Eagleson, 2007; Meng *et al.*, 2009). In bias momentum ADCS configurations, flywheel and magnetic coils are key devices, adjusting and maintaining satellite attitude to the desired orientation. In addition, a magnetometer is requisite, as its measurement provides the essential information in magnetic control torque calculations. With a flywheel, magnetic coils, and a magnetometer, a minimum bias momentum system can be set up. For pico-satellite, it is preferable that ADCS works properly without adding any new devices. Thus, a method of three-axis attitude determination using only magnetometer data is needed.

A number of previous efforts have addressed the problem of magnetometer-based three-axis attitude estimation (Psiaki *et al.*, 1990; Challa *et al.*, 2000; Psiaki and Oshman, 2003; Psiaki, 2004; Côté and Lafontaine, 2008; Hart, 2009). These algorithms all rely on accurate Euler models of the spacecraft dynamics and apply them with nonlinear filtering techniques, such as batch algorithm, nonlinear least square solver, extended Kalman filer (EKF), and square root unscented Kalman filter (SRUKF). These algorithms have been tested with flight data from several satellites, and have shown excellent performance. For pico-satellite operation, however, these on-board algorithms may not be suitable, as they may cause competition in computing resources allocation. As the pico-satellite's computing capacity is very limited while nonlinear estimation methods are always resource-consuming, implementing these algorithms may reduce the real-time processing capability of the satellite's on-board computer. A method has been reported recently for linearized magnetometer-based attitude estimation (Mimasu *et al.*, 2008). However, it only works when the satellite stabilizes its three-axis attitude, as it is the only condition in which the linearized dynamics/measurement equations can be used.

To fit the design restriction of a pico-satellite, this paper introduces a new magnetometer-based attitude estimation algorithm with linear filtering techniques. The algorithm is designed especially for cube-shaped bias momentum pico-satellites, in which a linear kinematics equation for satellite's pitch axis can be derived.

2 Linearized kinematics model

2.1 Bias momentum configuration

The simplified schematic configuration of a bias momentum pico-satellite is provided in Fig. 1. The reference coordinate of body axes is defined, where v represents satellite velocity. In this design, a spinning flywheel with angular momentum h_w is mounted on the orbit normal (or pitch) direction, and three-axis magnetic coils are installed separately on each axis. As a typical gyroscopic system, bias momentum control is a popular method for maintaining the stability of a spacecraft. The spinning flywheel creates a gyroscopic coupling between roll and yaw dynamics, which resists external disturbance and provides a basic stability in pitch axis (Bang *et al.*, 1997). The current through magnetic coils produces active control torque, which adjusts satellite attitude to the desired orientation (Silani and Lovera, 2005). Before the departure between pico-satellite and the launcher, the flywheel is accelerated to a high rotation speed. When the desired bias momentum is achieved, it remains constant. After separation, the magnetic coils are used to damp and stabilize the satellite. During the flight process, the spinning speed of the flywheel can be changed because of different control methods, but the desired bias momentum must be preserved to maintain the stability of satellite.

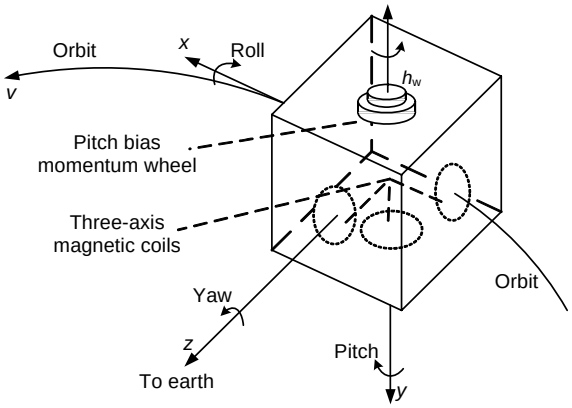

Fig. 1 Geometric configuration of a bias momentum pico-satellite

2.2 Attitude kinematics and dynamics model

Using the direct cosine matrix $\boldsymbol{A}$ to represent satellite attitude, the kinematics equation can be

written as

$$\dot{\boldsymbol{A}} = -[\boldsymbol{\omega}\times]\boldsymbol{A}, \tag{1}$$

$$[\boldsymbol{\omega}\times] = \begin{bmatrix} 0 & -\omega_z & \omega_y \\ \omega_z & 0 & -\omega_x \\ -\omega_y & \omega_x & 0 \end{bmatrix}, \tag{2}$$

where $\boldsymbol{\omega}$ is the inertial angular velocity of the pico-satellite expressed in the body fixed frame, and ω_x, ω_y, ω_z are its components.

For a rigid satellite with spinning flywheels, the attitude dynamics equation is

$$\dot{\boldsymbol{\omega}} = \boldsymbol{I}^{-1}[-[\boldsymbol{\omega}\times](\boldsymbol{I}\boldsymbol{\omega}+\boldsymbol{h}) - \dot{\boldsymbol{h}} + \boldsymbol{T}_c + \boldsymbol{T}_d], \tag{3}$$

where $\boldsymbol{I}$=diag$\{I_x, I_y, I_z\}$ is the moment of inertia, $\boldsymbol{T}_d$ is the disturbance torque, $\boldsymbol{T}_c$ is the control torque generated by magnetic coils, and $\boldsymbol{h}$ is the angular momentum of the flywheels. As there is only one flywheel installed on the pitch axis, $\boldsymbol{h}$=[0 h_y 0]. Then, the attitude motion of a bias momentum satellite is governed by the following equations:

$$\begin{cases} \dot{\omega}_x = \dfrac{1}{I_x}[(I_y - I_z)\omega_y\omega_z + h_y\omega_z + T_{cx} + T_{dx}], \\ \dot{\omega}_y = \dfrac{1}{I_y}[(I_z - I_x)\omega_z\omega_x - \dot{h}_y + T_{cy} + T_{dy}], \\ \dot{\omega}_z = \dfrac{1}{I_z}[(I_x - I_y)\omega_x\omega_y - h_y\omega_x + T_{cz} + T_{dz}], \end{cases} \tag{4}$$

where T_{cx}, T_{cy}, T_{cz} are the components of vector $\boldsymbol{T}_c$, and T_{dx}, T_{dy}, T_{dz} are the components of vector $\boldsymbol{T}_d$.

2.3 Assumptions for simplification

Momentum of inertia and bias momentum are two key parameters in designing a bias momentum system. Generally, significant coupling effects are achieved through large values of bias momentum. This implies that a condition may be imposed on the momentum (Kaplan, 1976).

$$|h_y| \gg \max(I_x\omega_o, I_y\omega_o, I_z\omega_o), \tag{5}$$

where ω_o is the orbital angular rate. To simplify the dynamics model of bias momentum satellite, Eq. (5) alone is not sufficient. Further assumptions must be made, according to the design speciality of pico-satellite.

Assumption 1 Moment of inertia is determined by the mass property and mechanical structure of a rigid body. As shown in Fig. 1, the pico-satellite has a symmetric cubic design structure, so it can be assumed that the diagonal elements of satellite's moment of inertia are almost equal with each other.

$$I_x \approx I_y \approx I_z. \tag{6}$$

Assumption 2 Magnetic coils can be used to reduce the satellite's angular velocity. According to the B-dot control law (Silani and Lovera, 2005), this damping procedure can be implemented without knowledge of satellite's attitude, so it is acceptable to operate an attitude estimation algorithm after damping, when the satellite's angular rate is considerably smaller. For bias momentum satellite, the result of B-dot damping control is that the body angular rate is approximately double the orbital angular rate.

$$|\boldsymbol{\omega}| \approx 2\omega_o. \tag{7}$$

2.4 General solution of the dynamics equation

With the conditions described in Eqs. (5)–(7), the X and Z axis equations of dynamics model (Eq. (4)) can be simplified by ignoring the minor parts.

$$\begin{cases} \dot{\omega}_x \approx \dfrac{h_y}{I_x}\omega_z + \dfrac{T_{cx}}{I_x} + \dfrac{T_{dx}}{I_x}, \\ \dot{\omega}_z \approx -\dfrac{h_y}{I_z}\omega_x + \dfrac{T_{cz}}{I_z} + \dfrac{T_{dz}}{I_z}. \end{cases} \tag{8}$$

These new differential equations represent a much simpler model. Generally, T_{cx}, T_{cz}, T_{dx}, T_{dz} and h_y all continue changing during the satellite's in-orbit flight; however, for a single control period, which might be several seconds, they can be seen as constants. Then, a general solution of Eq. (8) can be derived as follows:

$$\begin{cases} \omega_x = K_1 \sin\left(\dfrac{h_y}{\sqrt{I_x I_z}} t + \varphi\right) + \dfrac{T_{cz} + T_{dz}}{h_y}, \\ \omega_z = K_2 \cos\left(\dfrac{h_y}{\sqrt{I_x I_z}} t + \varphi\right) - \dfrac{T_{cx} + T_{dx}}{h_y}, \end{cases} \tag{9}$$

where K_1, K_2, and φ can be determined by the initial values of ω_x, ω_z, and t is the parameter of time. K_1, K_2 and φ only fit for one control period, where T_{cx}, T_{cz}, T_{dx}, T_{dz}, and h_y remain constant. For another control period, new values should be recalculated.

2.5 Linearized kinematics equation of satellite's pitch axis

As discussed in subsection 2.1, a pico-satellite with bias momentum has a basic stability in its pitch axis. Using $\boldsymbol{\alpha}$ to represents the satellite's pitch axis vector in inertial reference frame,

$$\boldsymbol{\alpha} = \boldsymbol{A}^{\mathrm{T}}[0 \quad 1 \quad 0]^{\mathrm{T}}. \tag{10}$$

A discrete kinematics model of vector $\boldsymbol{\alpha}$ can be derived as follows:

$$\begin{aligned} \boldsymbol{\alpha}_{k+1} &= \boldsymbol{A}_{k+1}^{\mathrm{T}}[0 \quad 1 \quad 0]^{\mathrm{T}} \\ &= [(1 - \Delta t[\boldsymbol{\omega}_k \times])\boldsymbol{A}_k]^{\mathrm{T}}[0 \quad 1 \quad 0]^{\mathrm{T}} \\ &= \boldsymbol{\alpha}_k + \boldsymbol{A}_k^{\mathrm{T}}[-\omega_{zk} \quad 0 \quad \omega_{xk}]^{\mathrm{T}} \Delta t, \end{aligned} \tag{11}$$

where Δt is the time interval between time k and time k+1.

In Eq. (9), the roll/yaw angular rate can be separated into two terms: a zero mean oscillatory term and an exterior torque response term. Correspondingly, in the kinematics Eq. (11), the attitude motion can be separated in two ways. The motion caused by the oscillatory angular velocity is the nutation motion, and the motion caused by the exterior torque response angular velocity is the attitude maneuver motion.

According to Assumption 2, the attitude estimation algorithm begins to operate after the damping procedure; thus, the amplitude K of the oscillatory term must be relatively small. Also, considering Eq. (5), the oscillation period is much smaller than the satellite orbit period. Generally, it is only tens of seconds. Therefore, the nutation motion of pico-satellite is weak and it does not change the orientation of pitch axis in a longer scope of time. With this conclusion, Eq. (11) can be further simplified as

$$\begin{aligned} \boldsymbol{\alpha}_{k+1} \approx \boldsymbol{\alpha}_k &+ h_y^{-1} \boldsymbol{A}_k^{\mathrm{T}}[-T_{cxk} \quad 0 \quad T_{czk}]^{\mathrm{T}} \Delta t \\ &+ h_y^{-1} \boldsymbol{A}_k^{\mathrm{T}}[-T_{dxk} \quad 0 \quad T_{dzk}]^{\mathrm{T}} \Delta t. \end{aligned} \tag{12}$$

3 Design of a linear estimation algorithm

The classic linear Kalman filter (KF) is an efficient recursive filter that estimates the state of a linear dynamic system from a series of noisy measurements. Since it only works with linear dynamics/measurements system, linear KF is seldom used in the problem of attitude estimation. The problem of estimating the attitude of a bias momentum pico-satellite, however, is a little different. In this special case, the kinematics equation (Eq. (12)) of satellite's pitch axis is linear, so it is possible to estimate the pitch axis orientation using a linear KF.

In this section, a linear KF based attitude estimation algorithm is introduced. The new algorithm has a coupling structure, consists of two modules: a linear KF module and a three-axis attitude determination method (TRIAD) module. After KF estimates the pitch axis orientation, the information of two different vectors, pitch axis vector and magnetic field vector, are both known, so the classic three-axis attitude determination algorithm TRIAD (Lerner, 1978) can be applied to calculate the final result.

3.1 Linear Kalman filter for pitch axis estimation

Eq. (12) can be written as

$$\boldsymbol{x}_k = \boldsymbol{x}_{k-1} + \boldsymbol{u}_{k-1} + \boldsymbol{w}_{k-1}, \tag{13}$$

$$\boldsymbol{u}_k = \boldsymbol{h}_y^{-1} \hat{\boldsymbol{A}}_k^{\mathrm{T}}[-T_{cxk} \quad 0 \quad T_{czk}]^{\mathrm{T}} \Delta t, \tag{14}$$

$$\boldsymbol{w}_k = h_y^{-1} \hat{\boldsymbol{A}}_k^{\mathrm{T}}[-T_{dxk} \quad 0 \quad T_{dzk}]^{\mathrm{T}} \Delta t, \tag{15}$$

where $\boldsymbol{x}_k$ is the filter's state vector, $\hat{\boldsymbol{A}}_k$ is the estimated attitude at time k, $\boldsymbol{u}_k$ is the system input, and $\boldsymbol{w}_k$ is the system error caused by disturbance. Generally, the disturbance torque $\boldsymbol{T}_{\mathrm{d}}$ can be approximated as zero mean Gaussian noise, then

$$E(\boldsymbol{w}_k)=0,\ E(\boldsymbol{w}_k\boldsymbol{w}_j^{\mathrm{T}})=\boldsymbol{Q}_k, \tag{16}$$

$$\boldsymbol{Q}_k=\hat{\boldsymbol{A}}_k^{\mathrm{T}}\mathrm{diag}\{\sigma_{\mathrm{d}}^2\quad 0\quad \sigma_{\mathrm{d}}^2\}\hat{\boldsymbol{A}}_k\Delta t^2/h_y^2, \tag{17}$$

where σ_{d} is the covariance of $\boldsymbol{T}_{\mathrm{d}}$, and represents the magnitude of the expected random disturbance.

From Eq. (10), we obtain

$$\boldsymbol{A}_k\boldsymbol{x}_k=[0\quad 1\quad 0]^{\mathrm{T}}. \tag{18}$$

Also, there is

$$\boldsymbol{B}_k=\boldsymbol{A}_k\boldsymbol{H}_k+\boldsymbol{\varepsilon}_{\mathrm{B}}, \tag{19}$$

where $\boldsymbol{B}_k$ is the measurement of the magnetic field by the magnetometer at time k, $\boldsymbol{H}_k$ is the corresponding value of the geomagnetic field with respect to the inertial reference frame, and $\boldsymbol{\varepsilon}_{\mathrm{B}}$ is the measurement noise vector. $\boldsymbol{\varepsilon}_{\mathrm{B}}$ is assumed to be a zero-mean Gaussian process with covariance $\boldsymbol{R}_k$.

From Eqs. (18) and (19), there is

$$y_k=B_{k2}=\boldsymbol{H}_k^{\mathrm{T}}\boldsymbol{x}_k+\varepsilon_{\mathrm{B2}}, \tag{20}$$

where B_{k2} is the second element of vector $\boldsymbol{B}_k$, and $\varepsilon_{\mathrm{B2}}$ represents the second elements of vector $\boldsymbol{\varepsilon}_{\mathrm{B}}$.

According to state vector $\boldsymbol{x}$, state model Eq. (13) and measurement model Eq. (20) are both linear; then, the classic linear KF can be applied. The equations of the filtering process are as follows:

$$\boldsymbol{x}_{k|k-1}=\boldsymbol{x}_{k-1}+\boldsymbol{u}_{k-1}, \tag{21}$$

$$\boldsymbol{P}_{k|k-1}=\boldsymbol{P}_{k-1}+\boldsymbol{Q}_{k-1}, \tag{22}$$

$$\boldsymbol{K}_k=\boldsymbol{P}_{k|k-1}\boldsymbol{H}_k^{\mathrm{T}}(\boldsymbol{H}_k\boldsymbol{P}_{k|k-1}\boldsymbol{H}_k^{\mathrm{T}}+\boldsymbol{R}_k)^{-1}, \tag{23}$$

$$\boldsymbol{x}_k=\boldsymbol{x}_{k|k-1}+\boldsymbol{K}_k(y_k-\boldsymbol{H}_k^{\mathrm{T}}\boldsymbol{x}_{k|k-1}), \tag{24}$$

$$\boldsymbol{P}_k=(\boldsymbol{I}_{3\times 3}-\boldsymbol{K}_k\boldsymbol{H}_k)\boldsymbol{P}_{k|k-1}, \tag{25}$$

where $\boldsymbol{P}$ is the state covariance matrix of KF, and $\boldsymbol{I}_{3\times 3}$ is the 3D identity matrix.

3.2 Attitude determination using TRIAD

After filtering, pitch axis vector and magnetic field vector are both known. Thus, it is convenient to compute the attitude matrix using the TRIAD algorithm.

In the TRIAD algorithm (Lerner, 1978), we constructed two triads of manifestly orthonormal reference and observation vectors according to

$$\begin{cases}\boldsymbol{r}_1=\boldsymbol{H}_k,\\ \boldsymbol{r}_2=(\boldsymbol{H}_k\times\boldsymbol{x}_k)/\left|\boldsymbol{H}_k\times\boldsymbol{x}_k\right|,\\ \boldsymbol{r}_3=(\boldsymbol{H}_k\times(\boldsymbol{H}_k\times\boldsymbol{x}_k))/\left|\boldsymbol{H}_k\times\boldsymbol{x}_k\right|,\\ \boldsymbol{s}_1=\boldsymbol{B}_k,\\ \boldsymbol{s}_2=(\boldsymbol{B}_k\times[0\quad 1\quad 0]^{\mathrm{T}})/\left|\boldsymbol{B}_k\times[0\quad 1\quad 0]^{\mathrm{T}}\right|,\\ \boldsymbol{s}_3=(\boldsymbol{B}_k\times(\boldsymbol{B}_k\times[0\quad 1\quad 0]^{\mathrm{T}}))/\left|\boldsymbol{B}_k\times[0\quad 1\quad 0]^{\mathrm{T}}\right|.\end{cases} \tag{26}$$

There exists a unique orthogonal matrix $\hat{\boldsymbol{A}}_k$ which satisfies

$$\hat{\boldsymbol{A}}_k\boldsymbol{r}_i=\boldsymbol{s}_i,\quad i=1,2,3, \tag{27}$$

given by

$$\hat{\boldsymbol{A}}_k=\sum_{i=1}^{3}\boldsymbol{s}_i\boldsymbol{r}_i^{\mathrm{T}}. \tag{28}$$

3.3 Coupling structure of the algorithm

A simple scheme of the suggested attitude estimation algorithm is shown in Fig. 2. Note that there is a coupling relationship between KF and TRIAD. The output of KF is used as the input of TRIAD, and the output of TRIAD feeds back to KF in the next filter step.

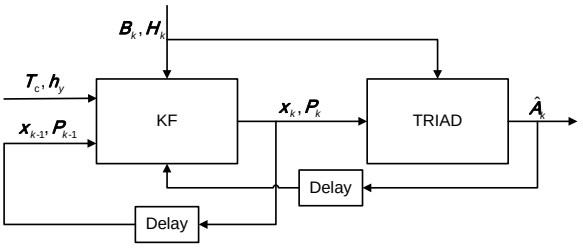

Fig. 2 Scheme of the suggested algorithm

Generally, as the feedback value may be inaccurate during the convergence process, a coupling structure may reduce filter performance in both accuracy and robustness. In this case, the feedback value is the KF system input $\boldsymbol{u}_k$, and it represents the control torque responding motion of satellite's pitch axis. Since the magnetic torque is relatively small,

and the bias momentum keeps the satellite's pitch axis stabilized, $\boldsymbol{u}_k$ only has a long period cumulative effect on variation of satellite's pitch axis. In a short period of time, the influence of $\boldsymbol{u}_k$ is very limited. Therefore, in initial convergence, even $\boldsymbol{u}_k$ might be inaccurate, the performance of KF remains unchanged. After the initial period, with KF converging, the accuracy of TRIAD module improves. This feeds back to KF, making its output more precise. Between KF and TRIAD, the relationship is symbiotic, and this refines the final result of the algorithm.

3.4 Tuning of the linear Kalman filter

The parameters $\boldsymbol{P}$, $\boldsymbol{R}$, and $\boldsymbol{Q}$ in the KF can be modified to optimize its performance for the given applications. Generally, filter tuning is one of the most difficult tasks in designing attitude estimation algorithms. It requires a deep understanding and extensive experience to select the correct parameters. Fortunately, the filter suggested in this study is a linear KF with less complexity, so it makes the task much easier.

From Eqs. (16), (17) and (19), the measurement covariance matrix $\boldsymbol{R}$ and the process noise covariance $\boldsymbol{Q}$ can be calculated. $\boldsymbol{R}$ equals to the magnetometer measurement covariance, which can be calculated from a prior test of the sensor; and $\boldsymbol{Q}$ is determined by random disturbance torque as well as current satellite attitude. The initial state covariance matrix $\boldsymbol{P}$ determines how fast the filter converges. In this application, a large $\boldsymbol{P}$ may cause the estimated state approach the actual state in several steps. This is very fast convergence, and also very risky. As there is not enough measurement information, the robustness of this convergence is not good, and the filter may diverge if some unexpected disturbance occurs. The suggested way in this study is to choose an arbitrarily small $\boldsymbol{P}$ which makes the filter converges in hundreds of steps. In this way, the robustness of the filter can be guaranteed, while the convergence time is still acceptable.

4 Numerical simulation results

4.1 Scenario definition

The cubic form pico-satellite in this simulation weights 2.5 kg, with a side length of 15 cm. As described in Fig. 1, three magnetic coils and one bias momentum flywheel are mounted inside satellite. Satellite's center of gravity is adjusted to its geometrical center. Table 1 lists the nominal values of the attitude dynamics.

Table 1 Attitude dynamic parameters of the pico-satellite

Parameter	Value	Parameter	Value
I_x (kg·m^2)	0.0111	h_y (N·ms)	−2.5
I_y (kg·m^2)	0.0119	h_z (N·ms)	0.01
I_z (kg·m^2)	0.0101	M_x (mA·m^2)	20
I_{xy}, I_{xz}, I_{yz} (kg·m^2)	0.0005	M_y (mA·m^2)	20
h_x (N·ms)	0.02	M_z (mA·m^2)	20

With the symmetric design structure, the diagonal elements of the moment of inertia I_x, I_y, and I_z are almost equal to each other, and the other elements are nearly zero. The flywheel is intended for installation on the pitch axis, but with some misalignment, the other two axes have momentum as well. M_x, M_y, and M_z are the maximum values of magnetic dipole for three-axis coils.

The orbit used in this simulation is a low earth orbit, with an altitude of 400 km and inclination of 70°. After separation from the launcher, the B-dot damp control is immediately applied, and the satellite's angular rate continues reducing until a certain level is reached. Then the prerequisite of the suggested attitude estimation algorithm is satisfied. The simulation begins with the initial angular velocity of satellite at [0.1 0.1 0.1] (°)/s, and the initial attitude of satellite is [10 100 10] (°). The large initial attitude error represents the satellite's tumble motion in the damping process.

During in-orbit flight, satellite attitude is controlled under three different control stages, i.e., the damping stage, the stable stage, and the free rotating control stage. Each stage takes 20000 simulation seconds. Fig. 3 shows the attitude variation in orbit reference frame. In the damping control stage, the satellite attitude is dominated by the B-dot control law, and the orientation of the satellite's pitch axis is slightly adjusted to orbit normal. In the stable control stage, the conventional PD control law (Silani and Lovera, 2005) is applied to maintain three-axis stabilization, and the pointing accuracy is within 5°. In the free rotating stage, the magnetic coils have no output,

and the satellite rotates freely due to disturbance torque.

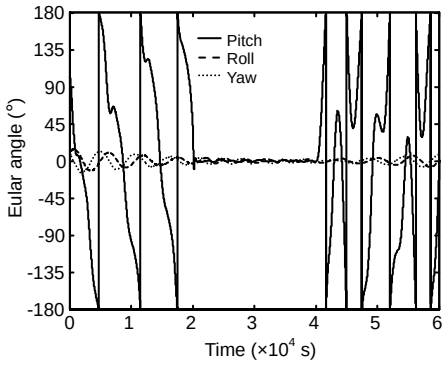

Fig. 3 Satellite attitude variation in orbit reference frame

4.2 Filter settings

To make the simulation more realistic, the following error sources were included:

1. Magnetometer measurement noise, 1σ= 0.5 mG.

2. Uncertainty in moment of inertia, about 5% (only the diagonal elements is used in the filter).

3. Misalignment in bias momentum, about 1% (momentum in roll and yaw axes is assumed zero in the filter).

4. Disturbance torque with amplitude up to 1×10^{-7} N·m.

5. Measurement bias of magnetic coils current and flywheel rotate speed, 2% of the measurement amplitude.

6. Magnetometer measurement bias, 3 mG on each axis.

7. Satellite position error, about 10 km in direct distance.

$\boldsymbol{R}$ of KF can be set as $(0.5\ \text{mG})^2$, and $\boldsymbol{Q}$ can be calculated by Eq. (17) with σ_d as about $1\times10^{-7}/3$ N·m. The initial parameters are given by

$$\boldsymbol{x}_{0\text{KF}}=[0\quad 1\quad 0]^{\text{T}}, \tag{29}$$

$$\boldsymbol{P}_{0\text{KF}}=1\times10^{-6}\boldsymbol{I}_{3\times3}. \tag{30}$$

Besides the KF-based algorithm, the EKF (Psiaki *et al.*, 1990) and the SRUKF (Côté and Lafontaine, 2008) are also tested. The filtering steps of all algorithms are unified at 5 s. State vectors of EKF and SRUKF are selected as $[\boldsymbol{q}\ \boldsymbol{\omega}]$, where $\boldsymbol{q}$ is the quaternion of satellite attitude. Differing from the original method (Psiaki *et al.*, 1990), the EKF in this simulation does not include constant disturbance torque $\boldsymbol{n}_\text{d}$ in state vector. This is because, in a cubic pico-satellite, magnetic torque is significantly larger than any other disturbance torque (Rankin, 2005), and with the satellite rotating, the magnetic disturbance changes greatly. As there is no stable constant in the disturbance torque, adding $\boldsymbol{n}_\text{d}$ to state vector does not improve filter performance. The EKF in this simulation is more or less similar to the estimation algorithm proposed by Appel (2005), when the satellite enters the shadow phase of its orbit.

For EKF and SRUKF, $\boldsymbol{Q}$ and $\boldsymbol{R}$ are set as magnitudes representative of the expected disturbance inputs and measurement noise, which are $(1\times10^{-7}/3$ N·m$)^2$ and $(0.5\ \text{mG})^2$. The initial parameters are given by

$$\boldsymbol{x}_{0\text{EKF}}=\boldsymbol{x}_{0\text{SRUKF}}=[0_{1\times3}\quad 1\quad 0_{1\times3}]^{\text{T}}, \tag{31}$$

$$\boldsymbol{P}_{0\text{EKF}}=\begin{bmatrix}0.3\boldsymbol{I}_{4\times4} & \boldsymbol{0}_{4\times3}\\ \boldsymbol{0}_{3\times4} & 0.001\boldsymbol{I}_{3\times3}\end{bmatrix}, \tag{32}$$

$$\boldsymbol{S}_{0\text{SRUKF}}=\text{Chol}(\boldsymbol{P}_{0\text{EKF}}), \tag{33}$$

where $\boldsymbol{S}_{0\text{SRUKF}}$ is the square-root matrix of the state covariance $\boldsymbol{P}_{0\text{EKF}}$ via a Cholesky factorization.

4.3 Filter performance

Fig. 4 shows the estimation result of KF state vector. Three components of the vector x_1, x_2, x_3 are shown respectively. The solid line represents the actual variation of satellite's pitch axis vector, and the dashed line represents the KF estimated value. In this figure, the dashed line approaches the solid line within about 100 steps (500 s), and then continues tracking it. The estimate error between two lines is within 0.04, and this error does not change during all three control stages.

To obtain a clearer view of the filter performance, a comparison of three algorithms is shown in Fig. 5. The filter estimation error θ in this figure is defined as axis angle between actual direct cosine matrix of satellite attitude $\boldsymbol{A}$ and estimated matrix $\hat{\boldsymbol{A}}$, which can be calculated by the following equation:

$$\theta = \arccos\left(\frac{1}{2}\left[\mathrm{tr}(\boldsymbol{A}\cdot\hat{\boldsymbol{A}}^{-1})-1\right]\right). \quad (34)$$

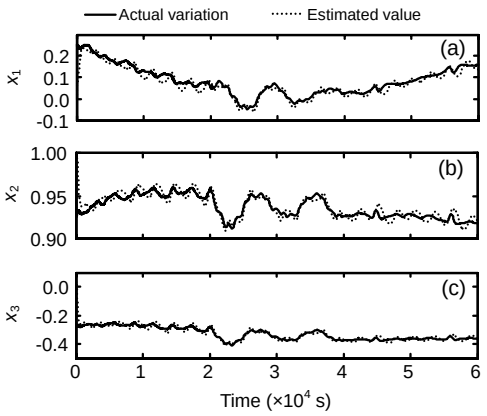

Fig. 4 Estimated result of KF state vector
(a) x_1, (b) x_2, and (c) x_3 components of vector $\boldsymbol{x}$

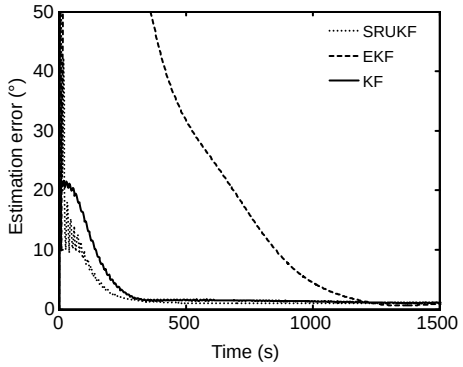

Fig. 5 Estimation results of KF, EKF, SRUKF during transient phase

For the KF-based algorithm, the estimated matrix is the output of TRIAD module; for EKF and SRUKF, the estimated matrix is calculated by the vector of estimated quaternion. In Fig. 5, three curves which represent EKF, SRUKF, and KF estimation errors converge to the same accuracy, within 3°. EKF and SRUKF are nonlinear filters based on the nonlinear dynamics/measurements equations, while the KF-based algorithm suggested in this study is a linear filter based on a linearized model. That KF has the same accuracy as EKF and SRUKF indicates that the simplified equation derived in subsections 2.3–2.5 describes attitude motion as well as the complete model in Eq. (3). The systematic error of this linear approximation is negligible and harmless in this scenario.

Although there is no significant difference in filter accuracy, diversity in convergence time can be easily found in Fig. 5. As there exists a large initial attitude error unknown to the filter, EKF converges the slowest, within about 2500 s, or 500 steps. SRUKF converges the fastest, within about 500 s, or 100 steps. Compared with EKF and SRUKF, the KF algorithm shows remarkable performance, the convergence time of KF is a little slower than that of SRUKF, but much faster than that of EKF. This result demonstrates the robustness and convergent ability of the KF algorithm. As discussed in subsection 3.4, with proper tuning of filter parameters, robustness of the KF algorithm can be guaranteed.

4.4 Error analysis

Attitude dynamics parameter errors and measurement biases are systematic errors. More or less, they will all affect filter accuracy. An analysis of these errors has been carried out for this case, and Table 2 summarizes the result. The method used to evaluate these effects is similar to the method introduced in Psiaki *et al.* (1990). With filter parameters unchanged, simulations were conducted using different dynamics/measurements models with each systematic error. The error analysis was computed with 1000 Monte Carlo simulation runs, and the average values of the error's state-time root mean square (RMS) are provided. In Table 2, there are only slightly differences in estimation errors between three filters. The accuracy of EKF is the highest, while the accuracy of KF is the lowest. Unexpectedly, the accuracy of SRUKF is lower than that of EKF. In a short sampling period, satellite dynamics model is fairly linear, and the advantage of UKF may not be revealed. Similar results can be seen in the comparison of EKF and UKF in orbit determination problem (Roh *et al.*, 2007), in which EKF also shows higher accuracy than UKF in short filtering steps. In this simulation, SRUKF only shows its superiority when there is only measurement noise in systematic errors. This result indicates that SRUKF approximates nonlinear dynamics better, when the system/measurement noise is pure Gaussian distribution. Also in that case, the result of KF with measurement noise alone is slightly better than that of EKF. This indicates that the linearized model introduced in this study has almost the same level of approximation as the method of EKF.

Table 2 Error analysis result

Error source	RMS value (°)		
	KF	EKF	SRUKF
1σ=0.5 mG magnetometer measurement noise	0.102	0.117	0.055
5% uncertainty in moment of inertia	0.059	0.049	0.055
1% misalignment in bias momentum	0.425	0.375	0.426
1×10^{-7} N·m amplitude disturbance torque	0.506	0.434	0.512
2% control torque measurement bias	0.033	0.015	0.021
3 mG magnetometer measurement bias on each axis	1.026	0.907	0.946
10 km satellite position error	0.676	0.679	0.678
Simulation with all errors	1.555	1.393	1.522

In Table 2, the main contributors to the errors are the measurement bias of magnetometer, as well as the calculation error of satellite position, which can also be understood as the magnetic field model error. As there is only one sensor in the system, the accuracy of magnetometer and magnetic field model has direct influence on the final filter performance. For further improvement, pre-flight or in-orbit magnetometer calibration (Crassidis *et al.*, 2005) may be used to achieve a higher estimation result. In addition to magnetic-related systematic errors, errors of flywheel misalignment and unknown disturbance also have some influence on filter performance. As relatively large bias momentum is needed to maintain satellite stability, its misalignment may cause problems in propagation of dynamics equations. For a low orbit cubic pico-satellite, magnetic torque which varies extensively with satellite rotating is the main part of disturbance (Rankin, 2005). A value of 1×10^{-7} N·m is relatively high, as satellite control torque is below 1×10^{-6} N·m (20 mA·m^2 max magnetic dipole and about 0.5 Gauss magnetic field). For filters, the unknown flywheel misalignment and disturbance torque can be considered as colored process noises. Simulation result shows that proper filter tuning may reduce the influence of these errors, providing the filter convergence with an acceptable accuracy and good robustness.

4.5 Computation burden test

The KF-based algorithm is a linear filtering method with a simplified model. Thus, it might consume significantly less computing resources compared with nonlinear filters. To find out how fast these filters run, a test was conducted by running them on a Texas Instruments (TI) digital signal processor (DSP) TMS320C5416, with a 20-MHz clock rate. Both KF and EKF are tested. UKF is not included, as it is already known that the computation time of UKF is generally three times longer than that of EKF (Roh *et al.*, 2007). Test software was programmed by C language. Results showed that EKF took six times more computing resources than the KF-based algorithm. For 1000 samples, it took about 22.0 s to operate EKF, while for the KF algorithm (KF plus TRIAD), the time was 2.9 s. Compared with nonlinear filters, the suggested KF-based algorithm consumes much less computing resources.

5 Conclusions

A linear KF-based algorithm for magnetometer-only attitude estimation problems is proposed in this paper. Compared with nonlinear estimation algorithms EKF and SRUKF, the method suggested in this paper shows remarkable performance in realistic simulations. The main features of the suggested algorithm are:

1. The algorithm consumes much less computing resources than nonlinear filters.

2. The algorithm has the same level of estimation accuracy as EKF and SRUKF.

3. The algorithm has the same level of rate of convergence as SRUKF.

4. The algorithm is applicable in all sorts of magnetic control stages.

Although the suggested algorithm has its particular advantages in magnetometer-only attitude estimation problems, there still exist some limitations:

1. The algorithm can only be used in cubic satellite with bias momentum configuration.

2. The algorithm can only be used after satellite's damping procedure.

3. The algorithm cannot directly estimate the information of satellite's angular rate.

Nevertheless, a magnetometer-only attitude estimation method for a low-altitude Earth orbit, bias momentum pico-satellite is achievable and remains advantageous compared to other methods.

References

Appel, P., 2005. Attitude estimation from magnetometer and earth-albedo-corrected coarse sun sensor measurements. *Acta Astronautica*, **56**(1-2):115-126. [doi:10.1016/j.actaastro.2004.09.001]

Bang, H., Kim, J.A., Kim, M., 1997. Optimal reorientation maneuver of bias momentum spacecraft. *Journal of Guidance, Control and Dynamics*, **20**(6):1076-1082. [doi:10.2514/2.4188]

Challa, M., Natanson, G., Ottenstein, N., 2000. Magnetometer-only Attitude and Rate Estimates for Spinning Spacecraft. Proceedings of the AIAA/AAS Astrodynamics Specialists Conference, Denver, CO, USA, p.311-321.

Côté, J., Lafontaine, J., 2008. Magnetic-only Orbit and Attitude Estimation Using the Square-root Unscented Kalman Filter Application to the PROBA-2 Spacecraft, Guidance, Navigation and Control Conference and Exhibit, Honolulu, Hawaii, USA.

Crassidis, J.L., Lai, K.L., Harman, R.R., Real-time attitude-independent three-axis magnetometer calibration. *Journal of Guidance, Control, and Dynamics*, **28**(1):115-120. [doi:10.2514/1.6278]

Eagleson, S., 2007. Attitude Determination and Control, Detailed Design, Test, and Implementation for CanX-2 and Preliminary Design for CanX-3 and CanX-45. MS Thesis, University of Toronto, Toronto, Canada.

Funase, R., Takei, E., Nakamura, Y., Nagai, M., Enokuchi, A., Chen, Y.L., Nakada, K., Nojiri, Y., Sasaki, F., Funane, F., *et al*., 2007. Technology demonstration on University of Tokyo's pico-satellite "XI-V" and its effective operation result using ground station network. *Acta Astronautica*, **61**(7-8):707-711. [doi:10.1016/j.actaastro.2006.12.032]

Harmann, R.J., Verhoeven, C.J.M., Bonnema, A.R., 2005. Nano-satellites, a Fast Way to Pre-qualify New Micro-Technology. International Conference on MEMS, NANO and Smart Systems, Banff, Alberta, Canada, p.263-264. [doi:10.1109/ICMENS.2005.80]

Hart, C., 2009. Satellite Attitude Determination Using Magnetometer Data Only. 47th AIAA Aerospace Sciences Meeting Including the New Horizons Forum and Aerospace Exposition, Orlando, Florida, USA.

Kaplan, M.H., 1976. Modern Spacecraft Dynamics and Control. John Wiley & Sons, New York, p.251.

Lerner, G.M., 1978. Three-axis Attitude Determination, Spacecraft Attitude Determination and Control. Wertz, J.R. (Ed.), D. Reidel, Dordrecht, the Netherlands, p.420-428.

Martinelli, M.I., Sánchez Peña, R.S., 2005. Passive 3 axis attitude control of MSU-1 pico-satellite. *Acta Astronautica*, **56**(5):507-517. [doi:10.1016/j.actaastro.2004.10.007]

Meng, T., Wang, H., Jin, Z.H., Han, K., 2009. Attitude stabilization of a pico-satellite by momentum wheel and magnetic coils. *Journal of Zhejiang University-SCIENCE A*, **10**(11):1617-1623. [doi:10.1631/jzus.A0820425]

Mimasu, Y., van der Ha, J.C., Narumi, T., 2008. Attitude Determination by Magnetometer and Gyros during Eclipse. AIAA/AAS Astrodynamics Specialist Conference and Exhibit, Honolulu, Hawaii, USA.

Nugent, R., Munakata, R., Chin, A., Coelho, R., Puig-Suari, J., 2008. CubeSat: The Pico-Satellite Standard for Research and Education, AIAA SPACE Conference and Exposition, San Diego, California, USA.

Psiaki, M.L., 2004. Global magnetometer-based spacecraft attitude and rate estimation. *Journal of Guidance, Control, and Dynamics*, **27**(2):240-250. [doi:10.2514/1.1039]

Psiaki, M.L., Oshman, Y., 2003. Spacecraft attitude rate estimation from geomagnetic field measurement. *Journal of Guidance, Control, and Dynamics*, **26**(2):244-252. [doi:10.2514/2.5065]

Psiaki, M.L., Martel, F., Pal, P.K., 1990. Three-axis attitude determination via Kalman filtering of magnetometer data. *Journal of Guidance, Control, and Dynamics*, **13**(3):506-514. [doi:10.2514/3.25364]

Rankin, D.J.P., 2005. Integration, Testing, and Operations of CanX-1 Picosatellite and the Design of the CanX-2 Attitude Determination and Control System. MS Thesis, University of Toronto, Toronto, Canada.

Roh, K.M., Park, S.Y., Choi, K.H., 2007. Orbit determination using the geomagnetic field measurement via the unscented Kalman filter. *Journal of Spacecraft and Rockets*, **44**(1):246-253. [doi:10.2514/1.23693]

Silani, E., Lovera, M., 2005. Magnetic spacecraft attitude control: a survey and some new results. *Control Engineering Practice*, **13**(3):357-371. [doi:10.1016/j.conengprac.2003.12.017]